Desmin intermediate filaments and tubulin detyrosination stabilize growing microtubules in the cardiomyocyte

Alexander K. Salomon[1], Naima Okami[1], Julie Heffler[1], Jia-Jye Lee[1], Patrick Robison[1], Alexey I. Bogush[1], Benjamin L. Prosser[1]

[1]Department of Physiology. Pennsylvania Muscle Institute. University of Pennsylvania Perelman School of Medicine. Philadelphia PA 19104

Abstract

The microtubule network of the cardiomyocyte exhibits specialized architecture, stability and mechanical behavior that accommodate the demands of working muscle cells. Stable, post-translationally detyrosinated microtubules are physical coupled to the sarcomere, the contractile apparatus of muscle, and resist sarcomere motion to regulate muscle mechanics and mechanosignaling. Control of microtubule growth and shrinkage dynamics represents a potential intermediate in the formation of a stable, physically coupled microtubule network, yet the molecular determinants that govern dynamics are unknown. Here we test the hypothesis that desmin intermediate filaments may stabilize growing microtubules at the sarcomere Z-disk in a detyrosination-dependent manner. Using a combination of biochemical assays and direct observation of microtubule plus-end dynamics in primary adult cardiomyocytes, we determine that: 1) tyrosination increases the frequency of microtubule depolymerization and reduces the pausing of microtubules at the Z-disk, leading to a more dynamic microtubule; and 2) desmin intermediate filaments stabilize both growing and shrinking microtubules specifically at the Z-

disk and protect them from depolymerization. This stabilizes iteratively growing, detyrosinated microtubules between adjacent sarcomeres, which promotes the formation of high-energy microtubules that buckle between sarcomeres and elevates myocyte viscoelasticity. Our findings inform on how the tubulin code and intermediate filaments regulate microtubule dynamics, and provide mechanism to the establishment of a spatially organized, physically coupled, and long-lived microtubule network in the cardiomyocyte.

Introduction

Microtubules are polymers of α- and β-tubulin that are characterized by cyclical transitions between polymerization and depolymerization, a behavior called dynamic instability[1]. Tuning this dynamic behavior confers unique functionality to specific sub-populations of microtubules[2]. Control of microtubule dynamics is cell type- and context-specific and can occur either by modulating polymer addition or subtraction at the ends, or through lateral interaction with the microtubule polymer[3]. The temporal and spatial control of dynamics can be tuned by post-translational modification of tubulin, which in turn affects the biophysical properties of the microtubule and interactions with microtubule associated proteins (MAPs)[4]. For example, detyrosination, the post translational removal of the C-terminal tyrosine residue on α-tubulin, has been shown to increase microtubule stability in mitotic cells by preventing their interaction with depolymerizing MAPs[5].

47 In the cardiomyocyte, microtubules fulfill both canonical roles in intracellular trafficking and
48 organelle positioning[6], as well as non-canonical functions matched to the unique demands of
49 working myocytes. In the interior of the myocyte, microtubules form a predominantly
50 longitudinal network that runs perpendicular to the transverse Z-discs that define the sarcomere,
51 the basic contractile unit of muscle (**Fig 1A**). Sub-populations of microtubules form physical
52 connections with the Z-disc that serve as lateral reinforcements along the length of the
53 microtubule[7]. Upon stimulation and sarcomere shortening, these physically coupled microtubules
54 buckle at short stereotypical wavelengths between sarcomeres to resist the change in myocyte
55 length[7]. The physical ramifications of these reinforced microtubules for the myocyte are
56 significant, as reinforced microtubules can resist 1000x more force than uncoupled
57 microtubules[8,9]. This viscoelastic resistance becomes particularly problematic in heart failure,
58 where proliferation of longitudinal, coupled microtubules stiffens the cardiomyocyte and impairs
59 myocyte motion[10].
60
61 Physical coupling of the microtubule to the sarcomere is tuned by detyrosination. Genetic
62 reduction of detyrosination by overexpression of tubulin tyrosine ligase (TTL), the enzyme
63 responsible for ligating the terminal tyrosine residue on detyrosinated tubulin, reduces
64 sarcomeric buckling and the viscoelastic resistance provided by microtubules, increasing
65 myocyte contractility[10]. Tyrosination status also governs microtubule-dependent
66 mechanotransduction in muscle that regulates downstream second messengers and is implicated
67 in myopathic states [11]. Given its ability to lower stiffness and improve the function of
68 myocardium from patients with heart failure[10], tyrosination is under pursuit as a novel

69 therapeutic approach. Yet how detyrosination promotes the interaction of microtubules with the
70 sarcomere to mediate their mechanical impact remains poorly understood.
71
72 Several observations suggest this interaction may be mediated at least in part through desmin
73 intermediate filaments that wrap around the Z-disk. Detyrosination promotes microtubule
74 interaction with intermediate filaments[7,12], and in the absence of desmin, microtubules are
75 disorganized and detyrosination no longer alters myocyte mechanics[7]. Additionally, a recent
76 pre-print indicates that intermediate filaments can directly stabilize dynamic microtubules in
77 vitro[13].
78
79 Despite this evidence, the effects of desmin or detyrosination on the dynamics of cardiomyocyte
80 microtubules have not been investigated. We hypothesized that desmin may serve to stabilize
81 growing microtubules at the Z-disk, which would represent an important intermediary in laterally
82 reinforcing the network and coupling microtubules to the sarcomere. Here, using a combination
83 of genetic manipulations, biochemical assays, and direct live-cell observation of dynamic
84 microtubules, we directly interrogated the effect of tyrosination status and desmin depletion on
85 microtubule dynamics. We find that desmin dictates the spatial organization of microtubule
86 dynamics and that growing microtubules are stabilized at the Z-disc in a desmin-dependent
87 fashion. Additionally, we find that tyrosinated microtubules are more dynamic, a characteristic
88 that precludes their ability to efficiently grow between adjacent sarcomeres and form stabilizing
89 interactions at the Z-disk. These findings provide insight into the organizing principles of
90 myocyte cytoarchitecture and into the mechanism of action for therapeutic strategies that target
91 detyrosinated microtubules.

92 **Results**

93

94 *Tyrosination alters the dynamics of the microtubule network*

95 We first sought to determine the effect of detyrosination on the dynamics of the cardiomyocyte
96 microtubule network. To reduce detyrosination, we utilized adenoviral delivery of TTL into
97 isolated adult rat cardiomyocytes[7]. TTL binds and tyrosinates tubulin in a 1:1 complex, and so
98 we also utilized adenoviral delivery of TTL-E331Q (E331Q), a verified catalytically dead mutant
99 of TTL[14], to separate effects of tubulin tyrosination from tubulin sequestration. We have
100 previously confirmed that TTL overexpression under identical conditions reduces detyrosination
101 below 25% of initial levels, while TTL-E331Q does not significantly affect detyrosination levels
102 with similar overexpression[14]. To specifically quantify the effects of reducing detyrosination on
103 the dynamic microtubule population, we adapted a subcellular fractionation assay from Fasset et
104 al., 2009[15] that allowed us to separate free tubulin from polymerized tubulin in the dynamic (i.e.
105 cold-sensitive) microtubule pool (**Fig 1B**).
106 Expression of TTL, but not E331Q, resulted in significantly less detyrosinated tubulin in the
107 dynamic microtubule pool (**Fig 1C**). Further, only TTL expression shifted tubulin away from the
108 polymerized fraction towards the free tubulin fraction, resulting in an increased ratio of free:
109 polymerized tubulin (**Fig 1C, S. Fig 1A**). This suggests that tyrosination effects the cycling of
110 tubulin within the dynamic microtubule pool. If indeed tyrosinated microtubules are more
111 dynamic, then levels of acetylation, a canonical marker of long-lived microtubules[16], should also
112 be decreased by TTL. Consistent with this, TTL, but not E331Q, led to a robust reduction in
113 levels of microtubule acetylation, suggesting that tyrosination reduces microtubule lifetime in the
114 cardiomyocyte (**Fig 1D**).

115 As acetylation itself is linked to microtubule stability[17,18], the TTL-dependent change in the
116 dynamic microtubule pool **(Fig 1C)** could be directly related to tyrosination or secondary to the
117 associated reduction in acetylation **(Fig 1D)**. To discriminate between these two hypotheses, we
118 directly modulated acetylation. To this end, we developed adenoviral constructs encoding
119 histone deacetylase 6 (HDAC6) and α tubulin acetyltransferase 1 (αTAT1). HDAC6 expression
120 reduced total microtubule acetylation to 25% of initial levels (**Fig 1E**) and αTAT1 expression
121 increased acetylation 12-fold (**Fig 1E**). Because αTAT1 has been shown to modulate
122 microtubule dynamics independent of enzymatic activity[19], we also used a pharmacological
123 inhibitor of HDAC6, Tubastatin A (TubA) to increase acetylation through an orthogonal
124 approach (**Fig 1E**). Having validated robust tools to modulate acetylation, we next determined
125 the effect of acetylation on the dynamic microtubule pool utilizing the same fractionation assay.
126 HDAC6 expression resulted in less acetylation in the cold-sensitive fraction while both αTAT1
127 expression and TubA treatment increased levels of acetylated tubulin. Neither genetic methods to
128 increase or decrease acetylation altered the free:polymerized tubulin (**Fig 1G, S. Fig 1B**);
129 however, TubA treatment modestly increased the free:polymerized tubulin ratio, suggesting that
130 while microtubule dynamics are likely unaffected by changing levels of acetylation, the presence
131 of HDAC6 protein may affect microtubule dynamics as observed previously[20]. Given that
132 modulating tyrosination altered levels of acetylation (**Fig 1D**), we also asked whether this
133 relationship was reciprocal. However, whole cell levels of detyrosination were largely
134 unaffected by modulating acetylation (**Fig 1F**), except for a modest increase with HDAC6
135 expression that may be related to HDAC6 association with microtubules increasing their stability
136 and availability for detyrosination[20].
137

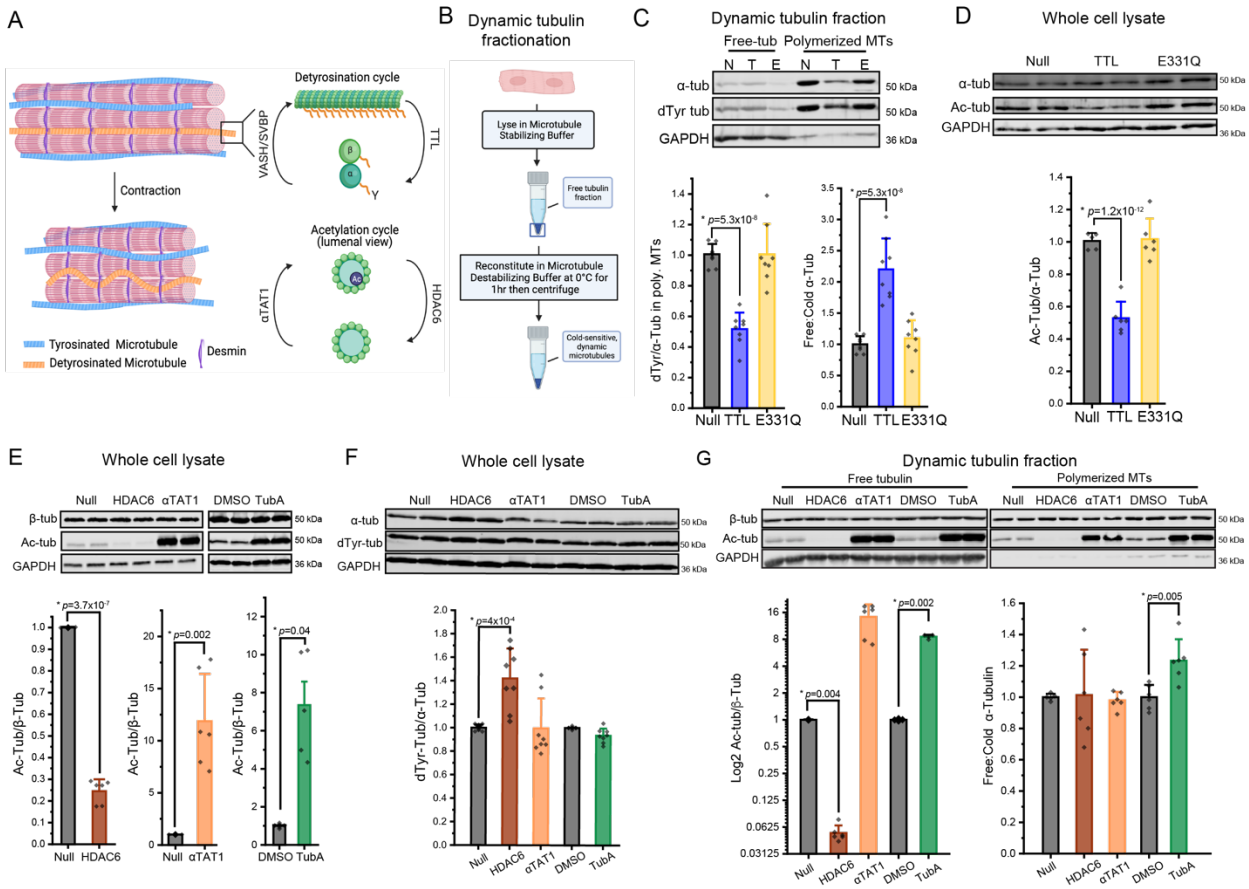

Figure 1. Tyrosination specifically alters microtubule stability. A Left, Schematic depicting detyrosinated microtubules (orange) buckling due to physical coupling with desmin at the Z-disc. Uncoupled tyrosinated microtubules (blue) do not buckle[7]. Right, Detyrosination and Acetylation cycles. **B** Overview of the cell fractionation assay adapted from Fasset et al. [15] that allows for separation of free tubulin and polymerized microtubules within the dynamic tubulin pool. **C** Representative western blot (**top**) and quantification (**bottom**) of α-tubulin, detyrosinated (dTyr) tubulin, and GAPDH in free and cold-sensitive microtubule fractions from adult rat cardiomyocytes infected with either null, TTL, or TTL-E331Q adenovirus. Detyrosinated tubulin values normalized to α-tubulin in cold-sensitive fraction. **D** Representative western blot (**top**) and quantification (**bottom**) of α-tubulin, acetylated tubulin, and GAPDH in whole-cell lysate from null, TTL, or E331Q expressing myocytes. **E** Validation of HDAC6 and αTAT1 constructs and Tubastatin a (TubA) treatment. Representative western blot (**top**) and quantification (**bottom**) of β-tubulin, acetylated tubulin, and GAPDH in whole-cell lysate from adult rat cardiomyocytes infected with HDAC6, αTAT1, or null adenovirus or treated with 1 μM TubA or DMSO overnight. **F** Representative western blot (**top**) and quantification (**bottom**) of α-tubulin, dTyr, and GAPDH in whole cell lysate from adult rat cardiomyocytes infected with HDAC6, αTAT1, or null adenovirus or treated with 1 μM TubA or DMSO overnight. **G** Representative western blot (**top**) and quantification (**bottom**) of β-tubulin, acetylated tubulin, and GAPDH in free and polymerized dynamic fractions. Lysate from myocytes infected with HDAC6, αTAT1, or null adenovirus or treated with 1 μM TubA or DMSO overnight. Western blot data points represent technical replicates (2 from each biological replicate) normalized to their respective controls (N=4 in C+F; N=3 in D, E, G). Statistical significance determined via two-sample T test with alpha adjusted for multiple comparisons. Data are presented as mean±SEM unless otherwise specified.

162 *Tyrosination increases catastrophes of growing microtubules*

163 We next wanted to more precisely quantify the effects of tyrosination on the dynamics of
164 individual microtubules. Microtubule dynamics (**Fig 2A)** are characterized by their rates of
165 growth (polymerization) and shrinkage (depolymerization) as well as the frequency of transitions
166 between these two states. Events are categorized as catastrophes (transitions from growth to
167 shrinkage), rescues (transitions from shrinkage to growth), and pauses (neither growth nor
168 shrinkage). We directly observed the microtubule plus-ends by time-lapse imaging of a
169 fluorescent end-binding protein 3 (EB3-GFP) construct expressed via adenovirus in isolated rat
170 cardiomyocytes (**S. Movie 1**). By creating kymographs from these videos, we were able to
171 quantify dynamic events (rescue, catastrophe, and pause) in addition to microtubule growth and
172 shrinkage kinetics (**Fig 2B)**. We harnessed off-target EB3-GFP Z-disc localization to
173 characterize dynamic events as occurring on or off the Z-disc, as in Drum et al.[21] As we noted
174 higher variability in measurements from one cell isolation to another than between cells from the
175 same isolation, experimental data were normalized to control data that were acquired from the
176 same animals.

177

178 We began with multiple control experiments. Although EB interaction is thought to be
179 unaffected by microtubule detyrosination[22], we wanted to validate that EB3 labeling of
180 microtubules did not systematically differ with TTL expression. EB3 fluorescence intensity
181 along the length and at the tip of the microtubule was unchanged in control, TTL or E331Q
182 expressing cells (**S. Fig 2A**), indicating that EB3 expression or labeling of microtubules was not
183 altered by our experimental interventions.

184

185 As adult ventricular cardiomyocytes are normally paced in vivo but quiescent in vitro, we sought
186 to determine whether electrical pacing and evoked contractions would overtly alter microtubule
187 dynamics. To this end, we timed the imaging of EB3 puncta to occur during the diastolic rest
188 interval between each contraction of cardiomyocytes that were electrically paced at 0.5Hz.
189 Internally controlled, pre- and post-comparisons of microtubule dynamics before and during
190 electrical stimulation showed no significant effect of stimulation on microtubule dynamic events
191 or growth kinetics in rat cardiomyocytes (**S. Fig 2B**). As such, for the remainder of this study we
192 interrogated quiescent cardiomyocytes to minimize movement artifacts.
193
194 Under basal conditions, we observed a stark spatial bias in microtubule dynamic behavior,
195 similar to that observed by Drum et al[21]. The initiation of microtubule growth, as well as pausing
196 of growth, predominantly occurred on the Z-disc (**Fig. 2C**). Conversely, catastrophes
197 predominantly occurred off the Z-disc, while rescue from catastrophe again occurred more
198 frequently at the Z-disc. As exemplified in **S. Movies 1-2**, in control (AdV-null) expressing
199 myocytes microtubules tend to grow iteratively from one Z-disk to another, often pausing at each
200 Z-disk region. If a microtubule undergoes catastrophe before reaching a Z-disk, it tends to shrink
201 to a previous Z-disk, where rescue is more likely to occur. These data suggest factors at the Z-
202 disc region strongly bias microtubule behavior and support the initialization as well as
203 stabilization of growing microtubules.
204
205
206
207

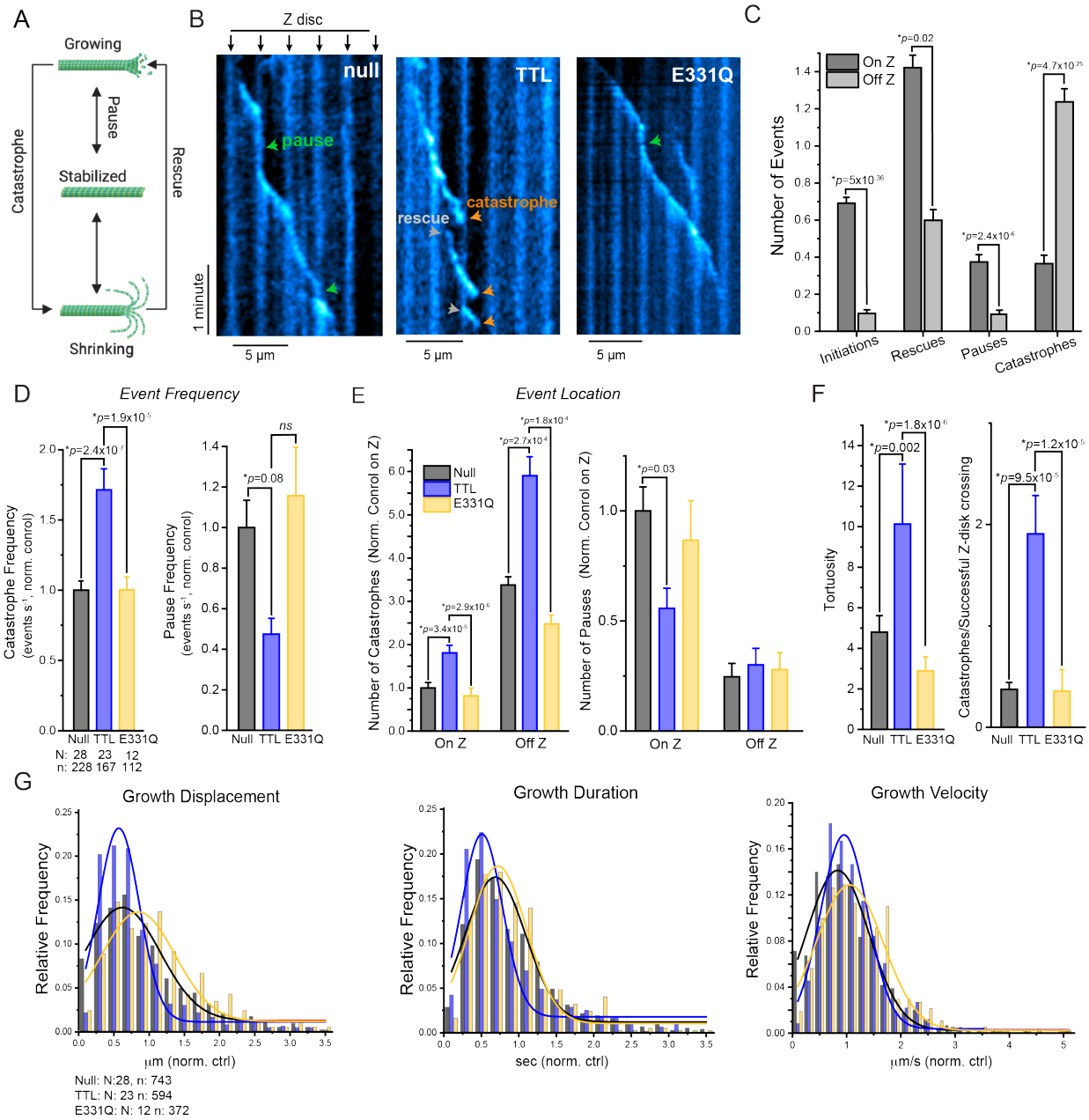

Figure 2 Tyrosinated microtubules are more dynamic A Schematic of microtubule dynamic events. **B** Representative kymographs from cardiomyocytes infected with EB3-GFP plus null, TTL or E331Q adenovirus. Arrowheads denote Z-discs. **C** Number of initiations, rescues, pauses, and catastrophes that occur on and off the Z-disc in isolated cardiomyocytes infected with null adenovirus. **D** Cell-wide catastrophe (**left**) and pause (**right**) frequency in myocytes infected with null, TTL, or E331Q adenovirus. **E** Number of catastrophes (**left**) and pauses (**right**) that occur on and off the Z-disc in myocytes infected with null (black), TTL (blue), or E331Q (yellow) adenovirus. **F** Gross measurements of microtubule dynamics. Tortuosity, the distance a microtubule grows divided by its displacement (**left**), and number of catastrophes in relation to number of successful Z-disk crossing (**right),** in myocytes infected with null, TTL, or E331Q adenovirus. **G** Frequency distribution of average microtubule growth displacement, duration, and velocity in myocytes infected with null, TTL, or E331Q adenovirus. Data are normalized to the average null value for the corresponding experiment. Statistical significance was determined with Kruskal-Wallis ANOVA with post-hoc test. Data are presented as mean±SEM unless otherwise specified.

222 We next interrogated the role of tyrosination. As seen in **S. Movie 3**, microtubules in TTL
223 treated cells also initiated growth at the Z-disk, but often had shorter runs and underwent
224 catastrophe prior to reaching a subsequent Z-disk. Consistently, TTL overexpression
225 significantly increased the frequency of catastrophes, while tending to reduce the frequency of
226 pausing (**Fig 2B and D**). E331Q expression did not alter event frequency **(S. Movie 4)**,
227 suggesting a tyrosination-specific effect on microtubule dynamics. Further examination of spatial
228 dynamics revealed that TTL similarly increased the number of catastrophes both on and off the
229 Z-disc while reducing the number of pauses specifically on the Z-disc (**Fig 2E**). As a readout of
230 inefficient growth, TTL increased microtubule tortuosity, the ratio of growth distance to growth
231 displacement (**Fig 2F**). Combined, the lack of stabilization at the Z-disc and more frequent
232 catastrophes resulted in tyrosinated microtubules breaking down ~4 fold as often before
233 successfully crossing a Z-disk when compared to either null or E331Q expressing cells (**Fig 2F**).
234 Consistent with an increased frequency of catastrophe, growth events in TTL myocytes were
235 shorter in duration and traveled less distance, despite similar growth velocity (**Fig 2G).** Of note,
236 cells expressing E331Q showed comparable growth metrics and event frequencies to control
237 infected myocytes, indicating that TTL's effect on microtubule dynamics is due to tyrosination
238 and not tubulin binding. Substantial overexpression of TTL or E331Q could reduce growth
239 velocity by limiting tubulin available for polymerization; we calculated the predicted effect of
240 our level of overexpression on tubulin growth velocity and found a negligible effect on growth
241 kinetics (**S. Fig 2D)**, consistent with our experimental observations (**Fig. 2G)**.
242
243
244

245 *Desmin structures the growing microtubule network*

246 We hypothesized that desmin intermediate filaments could be the Z-disc stabilizing factor for
247 growing microtubules, based in part on the gross microtubule misalignment observed in the
248 absence of desmin[23], and from our observation that microtubules tend to traverse the Z-disc at
249 desmin-enriched regions[10]. To determine if desmin regulates the dynamic population of
250 microtubules, we utilized the previously described fractionation assay **(Fig 1B)** with lysate from
251 rat cardiomyocytes infected with adenoviruses encoding shRNA against desmin (Des KD) or a
252 scramble control (scram). This construct has been previously validated to reduce desmin protein
253 levels ~70% under identical conditions[24]. Desmin depletion resulted in an increased free to
254 polymerized ratio in the dynamic microtubule pool (**Fig 3A, S. Fig 3A)**, suggesting that desmin
255 coordinates the stability of dynamic microtubules. We next quantified microtubule acetylation
256 and detyrosination, markers of long-lived microtubules, and found that both were decreased in
257 desmin depleted myocytes, without alterations in whole cell tubulin content (**Fig 3A**).
258

259 We next directly quantified plus-end microtubule dynamics by EB3-GFP upon desmin depletion.
260 As seen in **S. Movies 5-6**, upon desmin depletion microtubule growth still initiated at the Z-disk,
261 but the iterative, longitudinal growth from one Z-disk to another seen in control cells was lost.
262 Instead, microtubules often grew past Z-disk regions without pausing (**Fig 3B)**, and when
263 breaking down they were less likely to be rescued at the previous Z-disk. Blind quantification of
264 global event frequency revealed that desmin depletion modestly increased the frequency of
265 catastrophes while more robustly reducing both the frequency of rescues and pauses (**Fig 3C**).
266 Interrogation of where dynamic events occurred in relation to the Z-disk revealed that desmin
267 depletion specifically increased the number of catastrophes that occurred only on the Z-disk (**Fig**

268 **3D**), while reducing the number of catastrophes that occurred off the Z-disk. More strikingly,
269 desmin depletion markedly reduced the number of pauses and rescues that occur specifically on
270 the Z-disk, while not affecting pause or rescue behavior elsewhere (**Fig 3D**). Growth events
271 tended to travel longer distance with higher velocities in Des KD cells (**Fig 3E).** Together, these
272 results indicate that desmin is spatially coordinates microtubule dynamics and stabilizes both the
273 growing and shrinking microtubule at the Z-disk.
274
275 As the Z-disk region coordinates microtubule dynamics, we sought to summarize how our
276 different interventions (TTL, Desmin KD) affected the spatial organization of microtubule
277 behavior. By taking the ratio of events that occurred on vs. off the Z-disk and performing a log2
278 transform, we calculated a Z-disk bias for each type of dynamic event (**Fig 3F**). Of note, this
279 metric only reflects the spatial bias of events, not their frequencies. TTL reduced the preference
280 for microtubule pausing at the Z-disk, but did not affect the spatial preference of rescues,
281 catastrophes, or initiations (TTL increased catastrophe frequency in a spatially-agnostic fashion).
282 Desmin depletion, on the other hand, virtually eliminated any spatial preference of pausing,
283 rescue, or catastrophe behavior. Initiations had a strong Z-bias regardless of intervention, which
284 likely reflects nucleating events from microtubule organizing centers at Golgi outposts proximal
285 to the Z-disk that are not affected by these manipulations[25].
286
287
288
289
290

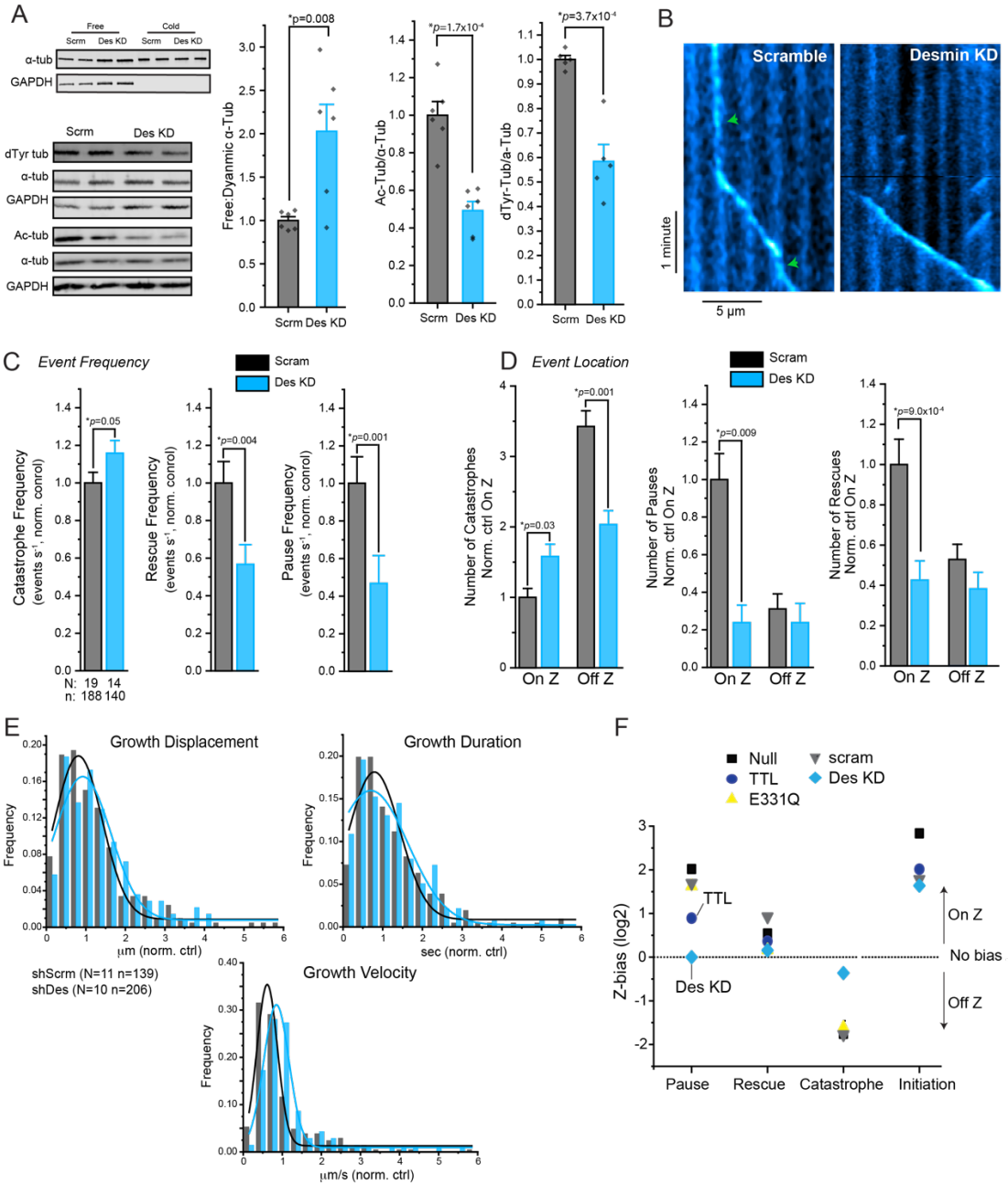

Figure 3 Desmin stabilizes the growing microtubule at the Z-disc A Representative western blot (**left**) and quantification (**right**) of α-tubulin, dTyr, acetylated tubulin, and GAPDH in free, cold-sensitive, or whole-cell lysate from isolated rat cardiomyocytes expressing either scramble (scrm) or desmin specific shRNA (Des KD). **B** Representative EB3-GFP kymograph from control or desmin KD myocytes. **C** Cell-wide catastrophe (**left**), rescue (**middle**), and pause (**right**) frequency with or without desmin KD. **D** Number of catastrophes (**left**), pauses (**middle**), and rescues (**right**) that occur on or off the Z-disc with or without desmin KD. **E** Frequency distribution of average microtubule growth displacement, duration, and velocity with or without desmin KD. **F.** Z-disc bias score (log2 transform of the ratio of events that occurred on vs. off the Z-disk) for all experimental conditions. Data are normalized to the average control value for the corresponding experiment. Statistical significance determined with Two Sample Kolmogorov-Smirnov Test. Data are presented as mean±SEM unless otherwise specified.

303

304 Cardiomyocytes from global, desmin germ-line knockout mice are characterized by misaligned
305 and degenerated sarcomeres[26] with a disorganized microtubule network [7]. Gross restructuring of
306 the myofilaments could affect microtubule dynamics due to a change in the physical
307 environment that is permissive to microtubule growth, for example by increasing the spacing
308 between Z-discs of adjacent myofilaments. To assess if our acute desmin depletion altered
309 myofilament spacing or alignment, we performed quantitative measurements on electron
310 micrographs from desmin depleted cardiomyocytes. Blind analysis indicated that acute desmin
311 depletion did not change myofilament spacing or alignment at this level of resolution (**S Fig 3B**),
312 consistent instead with a direct stabilizing effect of desmin intermediate filaments on the
313 microtubule network.

314

315 We next wanted to visualize the effect of desmin depletion on whole-cell microtubule network
316 organization. Airyscan imaging and blind image quantification indicated a reduction of the
317 percent cell area occupied by both detyrosinated and tyrosinated microtubules (**Fig 4A-B**),
318 consistent with reduced stability of microtubules upon desmin depletion. As a reduction in
319 detyrosinated microtubules and their association with the Z-disc is associated with reduced
320 cardiomyocyte viscoelasticity[7], we hypothesized that desmin-depleted myocytes would be less
321 stiff. To test this, we performed transverse nanoindentation of cardiomyocytes and quantified
322 Young's modulus of the myocyte over a range of indentation rates. Desmin depletion
323 specifically reduced the rate-dependent (viscoelastic) stiffness of the myocyte (**Fig 4C**), without
324 significantly altering rate-independent (elastic) stiffness. Reduced viscoelasticity is consistent
325 with reduced transient interactions between dynamic cytoskeletal filaments. To directly test if the

326 reduction in desmin alters microtubule buckling between sarcomeres, we performed a semi-
327 automated, blind analysis of microtubule buckling, as in our previous work[7]. In control cells,
328 most microtubules buckle in a clear sinusoidal pattern with a wavelength corresponding to the
329 distance of a contracted sarcomere (~1.5-1.9 μm) (**Fig 4D+G, S Movie 7**). Upon desmin
330 depletion, fewer polymerized microtubules were observed in general, with more chaotic
331 deformations and organization upon contraction (**S Movie 8**). For microtubules that did buckle,
332 the amplitude of buckles was reduced (**Fig. 4E**), as well as the proportion of microtubules that
333 buckled at wavelengths corresponding to the distance between 1 or 2 sarcomeres (1.5-1.9 or 3.0-
334 3.8 μm, respectively, **Fig 4F)**. Combined, these results are consistent with desmin coordinating
335 the physical tethering and lateral reinforcement of detyrosinated microtubules at the
336 cardiomyocyte Z-disk to regulate myocyte viscoelasticity.

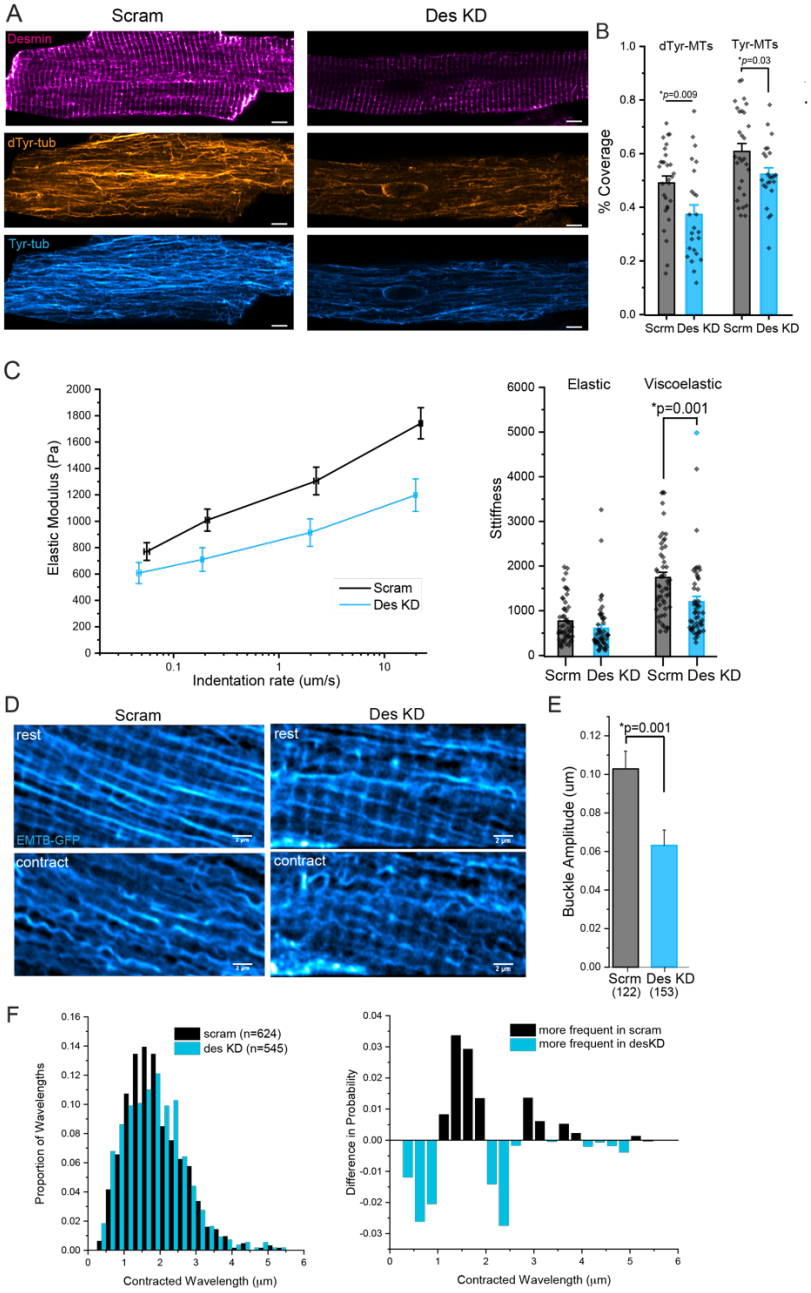

Figure 4 Desmin facilitates the microtubule contribution to viscoelastic resistance A. Representative Airyscan images of desmin (magenta), detyrosinated tubulin (orange), and tyrosinated tubulin (cyan) in isolated adult rat cardiomyocytes with or without desmin KD. **B** Quantification of percent cell area coverage of detyrosinated microtubules and tyrosinated microtubules with or without desmin KD. **C** Nanoindentation measurement of cardiomyocyte viscoelasticity. Left, Stiffness (elastic modulus) as a function of probe indentation velocity with or without desmin KD. Right, quantification of rate-dependent (viscoelastic) and independent (elastic) stiffness. **D** Representative images of microtubules in a cardiomyocyte at rest (top) and at the peak of contraction (bottom) with or without desmin KD. **E** Quantification of microtubule buckle amplitude. **F** Left, histogram of wavelength distribution of individual microtubule buckles. Right, distribution difference (scram – des KD from **G**). Statistical significance determined via 2-sided t test.

348

349 **Discussion**

350

351 In this paper we identify that 1) the dynamic, catastrophe-prone nature of tyrosinated
352 microtubules precludes their ability to faithfully grow to subsequent Z-discs; and 2) desmin
353 intermediate filaments structure and stabilize the growing microtubule network.

354

355 This study represents the first direct observation that tyrosination increases the dynamics of
356 cardiac microtubules. Increased dynamicity seems unlikely to arise from the PTM itself, [27] as the
357 C-terminal tyrosine is not believed to be critical involved in the formation of lateral contacts with
358 other tubulin dimers in the microtubule lattice. Yet, removal of this large hydrophobic residue
359 and subsequent exposure of acidic residues will alter hydrophobic and electrostatic interactions
360 on the outer surface of the polymerized microtubule. Through such a mechanism, tyrosination
361 can promote microtubule dynamics via increased interaction with destabilizing MAPs, or
362 through decreased interaction with stabilizing MAPs [27,28].

363

364 For example, detyrosination reduces the affinity of the depolymerizing kinesin MCAK for the
365 microtubule, increasing microtubule stability[5]. We hypothesized that increased MCAK affinity
366 may contribute to the increased rate of catastrophe we observed in tyrosinated microtubules; yet
367 due to its low abundance in the cardiomyocyte, our attempts to detect and knock down MCAK
368 levels were unreliable, precluding the immediate test of this hypothesis. The low abundance of
369 MCAK, while not ruling out a physiological rule, also motivates interrogation into alternative
370 stabilizing or destabilizing effector proteins.

371

372 Tyrosination status is also known to impact the recruitment of plus-end tip proteins (+Tips), such
373 as CLIP-170 and p150 glued[22], which may tune microtubule dynamics through either direct or
374 indirect effects. +Tip proteins also serve to couple the growing microtubule plus end with
375 cellular effectors[29]. In the search and capture mechanism, dynamic microtubules 'search' for sites
376 on the plasma membrane, chromosomes, and organelles to 'capture' via +Tip proteins[30]. The
377 interaction of microtubules with cellular structures, such as chromosomes or the cell cortex, has
378 been shown to promote rescue events through the formation of tension at the plus-end [31]. The
379 expression and localization of these proteins has been unexplored in the cardiomyocyte and
380 represents a potential mechanism for recognition of detyrosination- or intermediate filament-
381 dependent capture sites and the formation of durable detyrosinated microtubules.

382

383 We also identified that the intermediate filament desmin provides structure to the growing
384 microtubule network by stabilizing microtubules at the Z-disc. What is the mechanism of
385 desmin-dependent stabilization? A recent elegant *in vitro* study using reconstituted vimentin
386 intermediate filaments and microtubules indicates that intermediate filaments are sufficient to
387 stabilize growing microtubules through electrostatic and hydrophobic interactions[13]. The
388 interaction with intermediate filaments reduces catastrophes and promotes rescues, in strong
389 accordance with our *in cellulo* findings here. While MAPs may also be involved in modulating
390 microtubule-intermediate filament interactions, this direct effect is sufficient to explain the
391 primary phenotypes observed upon desmin depletion (i.e. increased catastrophes and reduced
392 pausing in the absence of desmin at the Z-disk, and a loss of Z-disk rescues).

393

394 The intermediate filament stabilization of growing microtubules would then provide a longer-
395 lived microtubule substrate to facilitate reinforcing, detyrosination-dependent interactions, such
396 as those previously documented between desmin and the microtubule through intermediates such
397 as Kinesin-1[32] or members of the plakin family of scaffolding proteins[33]. Desmin-mediated
398 interaction along the length of the microtubule may also lead to the loss of tubulin dimers at sites
399 of contact; these lattice defects are replaced by GTP-tubulin, which upon microtubule
400 catastrophe may function as a rescue sites[34]. Lateral interactions between microtubules and
401 intermediate filaments govern microtubule mechanical behavior upon compressive loading of
402 microtubules[9] allowing desmin to orchestrate microtubule buckling in the cardiomyocyte. [34]
403
404 Combined with past and current work, we propose a unifying model for microtubule-
405 intermediate filament interactions in the cardiomyocyte and how they contribute to myocardial
406 mechanics. Detyrosinated microtubules, with less frequent depolymerization, experience more
407 chance interactions with intermediate filaments at the Z-disc. The altered surface chemistry of
408 detyrosinated microtubules may also strengthen the electrostatic interactions with intermediate
409 filaments and additional cross-linking proteins. The periodic, lateral reinforcement of
410 microtubules increases their stability, leading to longer-lived microtubules and providing a
411 dynamic cross-link with the sarcomere, increasing the viscoelastic resistance to myocyte motion
412 and the ability of microtubules to transduce mechanical stress. Increased microtubule lifetimes
413 also promote microtubule acetylation, which itself increases the ability of microtubules to
414 withstand mechanical stress[35] and increases myocyte viscoelasticity[36]. In the setting of heart
415 disease, the increased abundance of both desmin intermediate filaments and detyrosinated

416 microtubules thus promotes a feed-forward substrate for enhanced mechanotransduction and
417 myocardial stiffening.
418
419
420 **Methods**
421
422 *Animals*
423 Animal care and procedures were approved and performed in accordance with the standards set
424 forth by the University of Pennsylvania Institutional Animal Care and Use Committee and the
425 Guide for the Care and Use of Laboratory Animals published by the US National institutes of
426 Health.
427
428 *Rat cardiomyocyte isolation and culture*
429 Primary adult ventricular myocytes were isolated from 6- to 8-week-old Sprague Dawley rats as
430 previously described[37]. Briefly, rats were anesthetized under isoflurane while the heart was
431 removed and retrograde perfused on a Lutgendorf apparatus with a collagenase solution. The
432 digested heart was then minced and triturated using a glass pipette. The resulting supernatant was
433 separated and centrifuged at 300 revolutions per minute to isolate cardiomyocytes that were
434 resuspended in rat cardiomyocyte media at a density that ensured adjacent cardiomyocytes did
435 not touch. Cardiomyocytes were cultured at 37°C and 5% CO_2 with 25 μmol/L of cytochalasin
436 D. The viability of rat cardiomyocytes upon isolation was typically on the order of 50-75% rod-
437 shaped, electrically excitable cells, and the survivability for 48hrs of culture is >80% (See
438 Heffler et al. [24]for our quantification of cardiomyocyte morphology in culture).

439

440 Rat cardiomyocyte media: medium 199 (Thermo Fisher 115090) supplemented with 1x Insulin-
441 transferrin-selenium-X (Gibco 51500056), 1 μg μl^{-1} primocin (Invivogen ant-pm-1), 20 mmol/L
442 HEPES at pH 7.4 and 25 μmol/L cytochalasin D.

443

444 *Fractionation assay of free tubulin and cold-sensitive microtubules*

445 Free tubulin was separated from cold-labile microtubules using a protocol adapted from Tsutusi
446 et al., 1993 and Ostlud et al., 1979. Isolated rat cardiomyocytes were washed once with PBS and
447 homogenized with 250 ul of microtubule stabilizing buffer using a tissue homogenizer. The
448 homogenate was centrifuged at 100,000 xg for 15 minutes at 25°C and the resulting supernatant
449 was stored at -80°C as the free tubulin fraction. The pellet was resuspended in ice-cold
450 microtubule destabilizing buffer and incubated at 0°C for 1 hour. After centrifugation at 100,000
451 xg for 15 minutes at 4°C the supernatant containing the cold-labile microtubule fraction was
452 stored at -80°C.

453

454 Microtubule stabilizing buffer: 0.5 mM $MgCl_2$, 0.5 mM EGTA, 10mM Na_3PO_4, 0.5 mM GTP,
455 and 1X protease and phosphatase inhibitor cocktail (Cell Signaling #5872S) at pH 6.95
456 Microtubule destabilizing buffer: 0.25 M sucrose, 0.5 mM $MgCl_2$ 10 mM Na_3PO_4, 0.5 mM GTP,
457 and 1X protease and phosphatase inhibitor cocktail (Cell Signaling #5872S) at pH 6.95

458

459 *Western blot*

460 For whole cell protein extraction, isolated rat cardiomyocytes were lysed in RIPA buffer
461 (Cayman #10010263) supplemented with protease and phosphatase Inhibitor cocktail (Cell

462 Signaling #5872S) on ice for 1 hour. The supernatant was collected and combined with 4X
463 loading dye (Li-COR #928-40004), supplemented with 10% 2-mercaptoethonol, and boiled for
464 10 minutes. The resulting lysate was resolved on SDS-PAGE gel and protein was blotted to
465 nitrocellulose membrane (Li-COR #926-31902) with mini Trans-Blot Cell (Bio-Rad).
466 Membranes were blocked for an hour in Odyssey Blocking Buffer (TBS) (LI-COR #927-50000)
467 and probed with corresponding primary antibodies overnight at 4 °C. Membranes were rinsed
468 with TBS containing 0.5% Tween 20 (TBST) three times and incubated with secondary
469 antibodies TBS supplemented with extra 0.2% Tween 20 for 1 hour at room temperature.
470 Membranes were washed again with TBST (0.5% Tween 20) and imaged on an Odyssey Imager.
471 Image analysis was performed using Image Studio Lite software (LI-COR). All samples were
472 run in duplicates and analyzed in reference to GAPDH.
473
474 *Antibodies and labels*
475 Acetylated tubulin; mouse monoclonal (Sigma T6793-100UL); western blot: 1: 1,000
476 Detyrosinated tubulin; rabbit polyclonal (Abcam ab48389); western blot: 1: 1,000
477 Alpha tubulin; mouse monoclonal, clone DM1A (Cell Signaling #3873); western blot: 1:1,000
478 Beta tubulin; rabbit polyclonal (Abcam ab6046); western blot: 1,000
479 Tyrosinated tubulin; mouse monoclonal (Sigma T9028-.2ML); Immunofluorescence: 1:1000
480 Desmin; rabbit polyclonal (ThermoFisher PA5-16705); western blot and immunofluorescence: 1:
481 1,000
482 GAPDH; mouse monoclonal (VWR GenScript A01622-40); western blot: 1:1,000
483 Goat anti-mouse AF 488 (1:1000 Life Technologies A11001)
484 Goat anti-rabbit AF 565 (1:1000 Life Technologies A11011)

485 IRDye 680RD Donkey anti-Mouse IgG (H + L) (LI-COR 926-68072); western blot: 1:10,000.

486 IRDye 800CW Donkey anti-Rabbit IgG (H + L) (LI-COR 926-32213); western blot: 1:10,000.

487

488 *Microtubule Dynamics by EB3*

489 Isolated rat cardiomyocytes were infected with an adenovirus containing an EB3-GFP construct.
490 After 48 hours, cells were imaged on an LSM Zeiss 880 inverted confocal microscope using a
491 40X oil 1.4 numerical aperture objective. Cells expressing EB3-GFP only at the tip were imaged
492 for four minutes at a rate of 1fps. Files were blinded, Gaussian blurred, and Z-compressed using
493 Image J (National Institutes of Health) to generate kymographs. The number of catastrophes,
494 rescues, and pauses were recorded per kymograph in addition to manual tracing of microtubule
495 runs to quantify time, distance, and velocity of microtubule growth or shrinkage. We refer to the
496 entire kymograph as the microtubule 'track' that is made up of individual growth and shrinkage
497 events we call 'runs'. Catastrophe and rescue frequency were calculated per cell by dividing the
498 number of catastrophes or rescues by total time spent in growth or shrinkage time, respectively.
499 Catastrophes and rescues occurring specifically on or off the Z-disc were normalized by the total
500 time of microtubule growth and shrinkage. Experimental values were normalized to their
501 respective control cells (Null for TTL and E331Q, or shScrm for shDes) acquired from the same
502 animals. A minimum of 3 separate cell isolations were performed for each group.

503

504 *Immunofluorescence*

505 Cells were fixed in pre-chilled 100% methanol for 8 minutes at -20°C. Cells were washed 4x
506 then blocked with Sea Block Blocking Buffer (abcam #166951) for at least 1 hour followed by
507 antibody incubation for 24-48 hours. Incubation was followed by washing 3x with Sea Block,

508 then incubated with secondary antibody for 1 hour. Fixed cells were mounted using Prolong
509 Diamond (Thermo #P36961)
510 We used ImageJ to calculate the percent area fraction of both desmin and microtubules. An ROI
511 was drawn to include the entire cell boundary minus the nucleus. For each image we identified
512 the percent fractional coverage of a fluorescence signal over a manually identified threshold as
513 described previously[10].
514
515 *Buckling analysis*
516
517 Adult rat cardiomyocytes were isolated as previously described and infected with adenovirus
518 carrying the microtubule-binding protein EMTB chimerically fused to 3 copies of GFP. The
519 purpose of this construct was to label microtubules fluorescently for imaging. The cells were
520 allowed 48 hours to express the construct. All cells chosen were those that contained sufficient
521 brightness and contrast to observe microtubule elements and where the health of the myocyte
522 was not compromised. To interrogate microtubule buckling amplitude and wavelength, cells
523 were induced to contract at 1 Hz 25 V and imaged during the contraction. For analysis, images
524 were blinded, and a microtubule was located that could be followed during the contraction. The
525 backbone was manually traced at rest and during its peak of contraction and the ROI was saved.
526 The ROI was then analyzed using a macro that rotated so that the ROI had the peak of
527 contraction 90 degrees to the axis of contraction to protect from aliasing errors. The program
528 then calculated the distance between the axis of the ROI and its peak and calculated the peak
529 (amplitude) and the width (half wavelength).
530
531 *Electron Microscopy*

532 Transmission electron microscopy images were collected as previously described [24]. Images at
533 7500x were rotated so the cells were parallel to the longitudinal axis. ROIs were generated
534 between adjacent Z-discs to quantify sarcomere spacing and the angle relative to 90°.
535
536 *Statistics*
537 Statistical analysis was performed using OriginPro (Version 2018). Normality was determined
538 by Shapiro-Wilk test. For normally distributed data, two sample t-test or one-way ANOVA was
539 utilized as appropriate. For non-normally distributed data, two sample Kolmogrov-Smirnov test
540 or Kruskal-Wallis ANOVA was utilized as appropriate. Specific statistical tests and information
541 of biological and technical replicates can be found in the figure legends. Unless otherwise noted,
542 'N' indicates the number of cells analyzed and 'n' indicates number of microtubule runs.
543
544
545
546
547
548
549
550
551

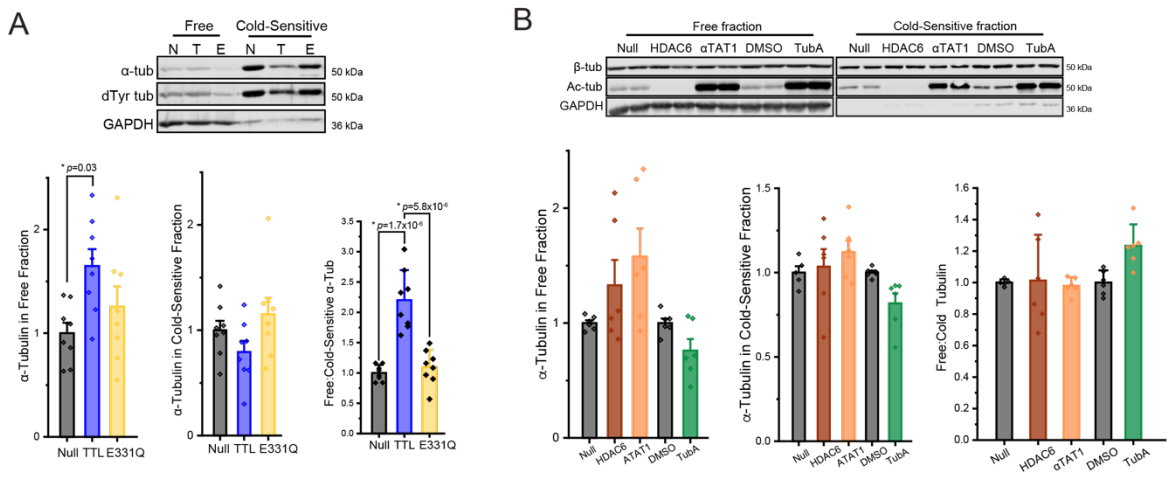

S. Figure 1. Supplemental figures associated with figure 1. A Representative western blot (**top**) and quantification (**bottom**) for α-tubulin, dTyr tubulin, and GAPDH in free and cold-sensitive fractions from rat cardiomyocytes infected with null, TTL, or E331Q adenovirus. **B** Representative western blot (**top**) and quantification (**bottom**) for α-tubulin, dTyr tubulin, and GAPDH in free and cold-sensitive fractions from rat cardiomyocytes either infected with null, HDAC, or ATAT1 adenovirus or treated with DMSO or TubA. Statistical significance determined via ANOVA with post hoc Bonferroni test.

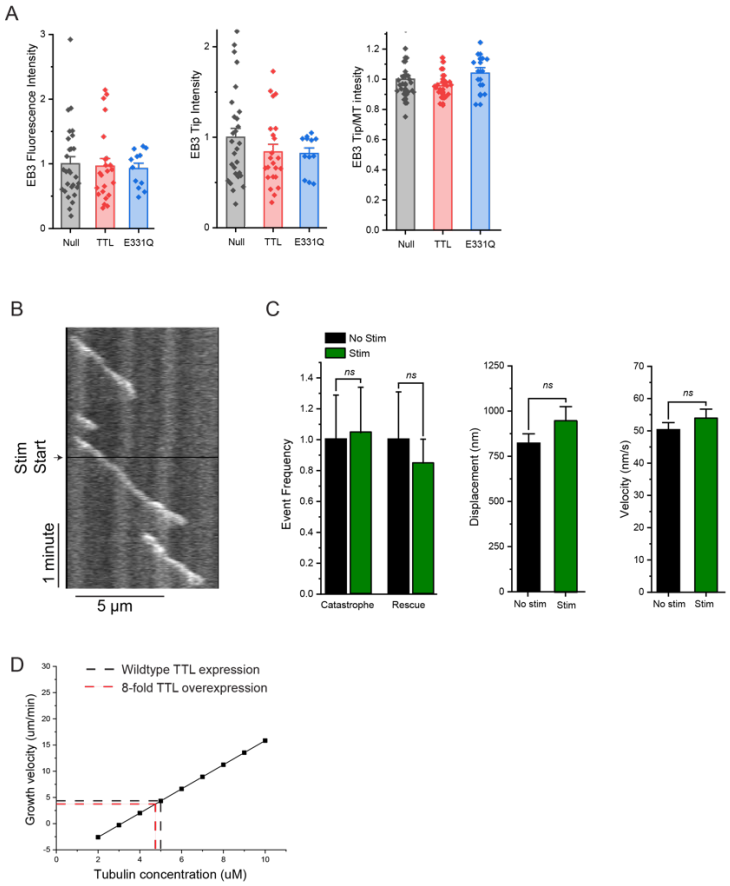

S. Figure 2. Supplemental figures associated with figure 2. A Background (**left**) EB3-GFP fluorescence intensity, EB3 tip fluorescence intensity (**center**) and the ratio of EB3 tip fluorescence intensity to microtubule EB3 intensity (**right**) in isolated rat cardiomyocytes co-infected with null, TTL, or E331Q adenovirus. Statistical significance determined via ANOVA with post hoc Bonferroni test. **B** Representative EB3-GFP kymograph from isolated rat cardiomyocyte before and after 0.5 Hz electrical stimulation. **C** Quantification of catastrophe frequency, rescue frequency, microtubule growth displacement and growth velocity before and after electrical stimulation. **D** To reduce levels of detyrosination in this study we relied on overexpression of TTL, which is known to associate with the free α/β tubulin heterodimer in a 1:1 complex with a K_d of 1 μM[38]. Due to the nature of this interaction, TTL overexpression can decrease the amount of "polymerization-competent" tubulin, leading to a decrease of *in vitro* microtubule polymerization[38]. The relationship between free tubulin concentration and microtubule polymerization is described as a simple 1D model below, where v_g is the velocity of microtubule growth, *d* is the dimer length (assumed to be 8 nm), k_{on} is the tubulin dimer association constant per protofilament (assumed to be 4.8 $\mu M^{-1}s^{-1}$)[30], k_{off} is the tubulin dissociation rate constant per protofilament (assumed to be $15s^{-1}$)[30] , and [Tb] is the concentration of free tubulin[39].

$$v_g = d\left(k_{on}[Tb] - k_{off}\right).$$

Solving for the equation of the line at a physiologic tubulin concentration of 5μM provides a theoretical value of 4.32 μm s^{-1} for growth velocity. Using the K_d value for TTL-tubulin interaction at a tubulin concentration of 5μM suggests that an 8-fold overexpression of TTL [14]will produce 0.2 μM of TTL-tubulin complex. If we assume that tubulin bound to TTL cannot be polymerized, then only 4.8 μM of free tubulin is polymerization-competent at any time. This change in polymerization-competent tubulin would lead to ~10% decrease in growth velocity. We did not observe an effect of E331Q on microtubule growth kinetics or on event frequency suggesting that the local tubulin concentration at the microtubule plus-tip is unaffected by the sequestration activity of TTL. Statistical significance determined via 2-sided t test.

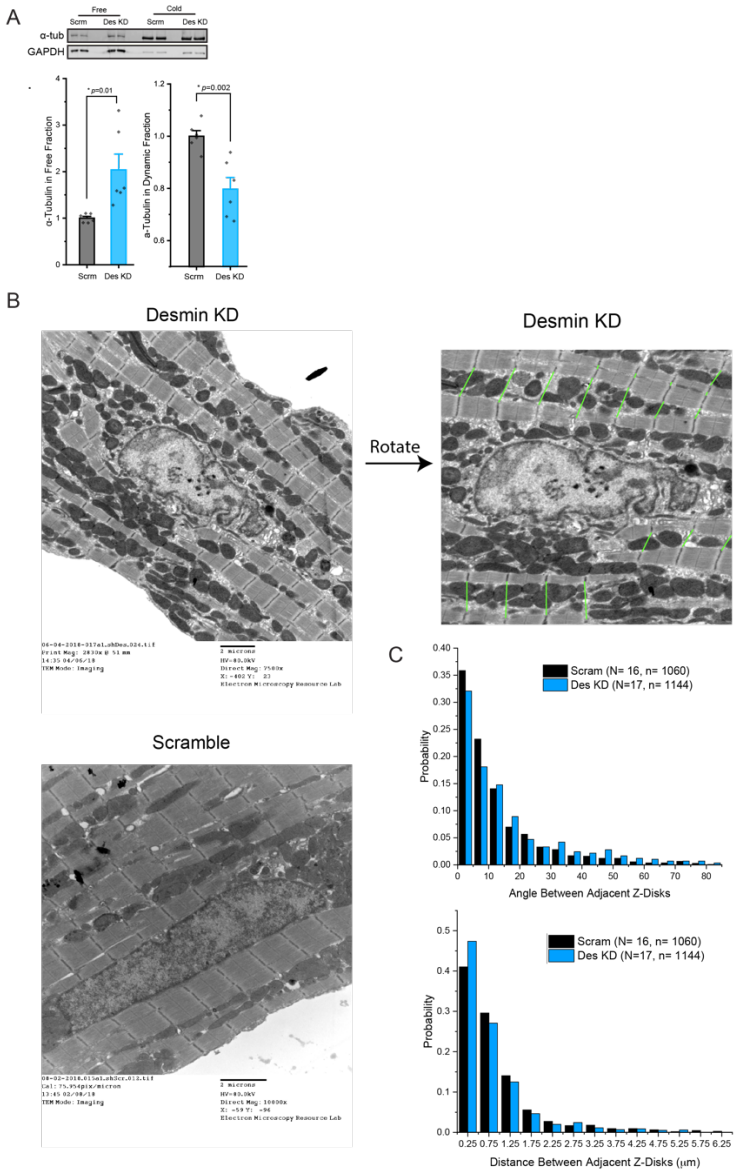

S. Figure 3. Supplemental figures associated with figure 3. A Representative western blot (**top**) and quantification (**bottom**) for α-tubulin and GAPDH in free and cold-sensitive fractions from rat cardiomyocytes infected with adenovirus containing scramble shRNA (scrm) or shRNA for desmin (Des KD). **B** Representative electron microscopy images of isolated rat cardiomyocytes with or without desmin knockdown. **C** Probability density plot of angle (**top**) and distance (**bottom**) between adjacent Z-discs with or without desmin knockdown.

607 **Acknowledgements**

608 The authors thank Matthew Caporizzo for providing the script used to quantify IF fractional

609 coverage and Tim McKinsey for the HDAC6 and αTAT1 constructs.

610

611 **Competing interests**

612 The authors declare no competing interests.

613

614 **References**

615

616 1. Mitchison, T. & Kirschner, M. Dynamic instability of microtubule growth. *Nature* **312**, 237–
617 242 (1984).

618 2. Forges, H. de, Bouissou, A. & Perez, F. Interplay between microtubule dynamics and
619 intracellular organization. *Int J Biochem Cell Biology* **44**, 266–274 (2012).

620 3. Akhmanova, A. & Steinmetz, M. O. Control of microtubule organization and dynamics: two
621 ends in the limelight. *Nat Rev Mol Cell Bio* **16**, 711–726 (2015).

622 4. Roll-Mecak, A. How cells exploit tubulin diversity to build functional cellular microtubule
623 mosaics. *Curr Opin Cell Biol* **56**, 102–108 (2019).

624 5. Peris, L. *et al*. Motor-dependent microtubule disassembly driven by tubulin tyrosination. *J*
625 *Cell Biology* **185**, 1159–1166 (2009).

626 6. Caporizzo, M. A., Chen, C. Y. & Prosser, B. L. Cardiac microtubules in health and heart
627 disease. *Exp Biol Med* **244**, 1255–1272 (2019).

628 7. Robison, P. *et al*. Detyrosinated microtubules buckle and bear load in contracting
629 cardiomyocytes. *Science* **352**, aaf0659 (2016).

630 8. Brangwynne, C. P. *et al*. Microtubules can bear enhanced compressive loads in living cells
631 because of lateral reinforcement. *J Cell Biology* **173**, 733–741 (2006).

632 9. Soheilypour, M., Peyro, M., Peter, S. J. & Mofrad, M. R. K. Buckling Behavior of Individual
633 and Bundled Microtubules. *Biophys J* **108**, 1718–1726 (2015).

634 10. Chen, C. Y. *et al*. Suppression of detyrosinated microtubules improves cardiomyocyte
635 function in human heart failure. *Nat Med* **24**, 1225–1233 (2018).

636 11. Kerr, J. P. *et al*. Detyrosinated microtubules modulate mechanotransduction in heart and
637 skeletal muscle. *Nat Commun* **6**, 8526 (2015).

638 12. Gurland, G. & Gundersen, G. G. Stable, detyrosinated microtubules function to localize
639 vimentin intermediate filaments in fibroblasts. *J Cell Biology* **131**, 1275–1290 (1995).

640 13. Schaedel, L., Lorenz, C., Schepers, A. V., Klumpp, S. & Köster, S. Vimentin Intermediate
641 Filaments Stabilize Dynamic Microtubules by Direct Interactions. *Biorxiv* 2020.05.20.106179
642 (2021) doi:10.1101/2020.05.20.106179.

643 14. Chen, C. Y. *et al*. Depletion of Vasohibin 1 Speeds Contraction and Relaxation in Failing
644 Human Cardiomyocytes. *Circ Res* **127**, e14–e27 (2020).

645 15. Fassett, J. T. *et al*. Adenosine regulation of microtubule dynamics in cardiac hypertrophy. *Am*
646 *J Physiol-heart C* **297**, H523–H532 (2009).

647 16. Webster, D. R. & Borisy, G. G. Microtubules are acetylated in domains that turn over slowly.
648 *J Cell Sci* **92 (Pt 1)**, 57–65 (1989).

649 17. Eshun-Wilson, L. *et al*. Effects of α-tubulin acetylation on microtubule structure and
650 stability. *Proc National Acad Sci* **116**, 201900441 (2019).

651 18. Xu, Z. *et al*. Microtubules acquire resistance from mechanical breakage through intralumenal
652 acetylation. *Science* **356**, 328–332 (2017).

653 19. Kalebic, N. *et al*. Tubulin Acetyltransferase αTAT1 Destabilizes Microtubules Independently
654 of Its Acetylation Activity. *Mol Cell Biol* **33**, 1114–1123 (2013).

655 20. Asthana, J., Kapoor, S., Mohan, R. & Panda, D. Inhibition of HDAC6 Deacetylase Activity
656 Increases Its Binding with Microtubules and Suppresses Microtubule Dynamic Instability in
657 MCF-7 Cells*. *J Biol Chem* **288**, 22516–22526 (2013).

658 21. Drum, B. M. L. *et al*. Oxidative stress decreases microtubule growth and stability in
659 ventricular myocytes. *J Mol Cell Cardiol* **93**, 32–43 (2016).

660 22. Peris, L. *et al*. Tubulin tyrosination is a major factor affecting the recruitment of CAP-Gly
661 proteins at microtubule plus ends. *J Cell Biology* **174**, 839–849 (2006).

662 23. Watkins, S. C., Samuel, J. L., Marotte, F., Bertier-Savalle, B. & Rappaport, L. Microtubules
663 and desmin filaments during onset of heart hypertrophy in rat: a double immunoelectron
664 microscope study. *Circ Res* **60**, 327–336 (2018).

24. Heffler, J. *et al*. A Balance Between Intermediate Filaments and Microtubules Maintains Nuclear Architecture in the Cardiomyocyte. *Circ Res* **126**, e10–e26 (2020).

25. Oddoux, S. *et al*. Microtubules that form the stationary lattice of muscle fibers are dynamic and nucleated at Golgi elementsSkeletal muscle microtubule dynamics. *J Cell Biology* **203**, 205–213 (2013).

26. Brodehl, A., Gaertner-Rommel, A. & Milting, H. Molecular insights into cardiomyopathies associated with desmin (DES) mutations. *Biophysical Rev* **10**, 983–1006 (2018).

27. Webster, D. R., Wehland, J., Weber, K. & Borisy, G. G. Detyrosination of alpha tubulin does not stabilize microtubules in vivo. *J Cell Biology* **111**, 113–122 (1990).

28. Khawaja, S., Gundersen, G. G. & Bulinski, J. C. Enhanced stability of microtubules enriched in detyrosinated tubulin is not a direct function of detyrosination level. *J Cell Biology* **106**, 141–149 (1988).

29. Kumar, P. & Wittmann, T. +TIPs: SxIPping along microtubule ends. *Trends Cell Biol* **22**, 418–428 (2012).

30. Mimori-Kiyosue, Y. & Tsukita, S. "Search-and-Capture" of Microtubules through Plus-End-Binding Proteins (+TIPs). *J Biochem* **134**, 321–326 (2003).

31. Gardner, M. K., Zanic, M. & Howard, J. Microtubule catastrophe and rescue. *Curr Opin Cell Biol* **25**, 14–22 (2013).

32. Liao, G. & Gundersen, G. G. Kinesin Is a Candidate for Cross-bridging Microtubules and Intermediate Filaments SELECTIVE BINDING OF KINESIN TO DETYROSINATED TUBULIN AND VIMENTIN*. *J Biol Chem* **273**, 9797–9803 (1998).

33. Favre, B. *et al*. Plectin interacts with the rod domain of type III intermediate filament proteins desmin and vimentin. *Eur J Cell Biol* **90**, 390–400 (2011).

34. Aumeier, C. *et al*. Self-repair promotes microtubule rescue. *Nat Cell Biol* **18**, 1054–1064 (2016).

35. Portran, D., Schaedel, L., Xu, Z., Théry, M. & Nachury, M. V. Tubulin acetylation protects long-lived microtubules against mechanical ageing. *Nat Cell Biol* **19**, 391–398 (2017).

36. Coleman, A. K., Joca, H. C., Shi, G., Lederer, W. J. & Ward, C. W. Tubulin acetylation increases cytoskeletal stiffness to regulate mechanotransduction in striated muscle. *J Gen Physiol* **153**, e202012743 (2021).

37. Prosser, B. L., Ward, C. W. & Lederer, W. J. X-ROS Signaling: Rapid Mechano-Chemo Transduction in Heart. *Science* **333**, 1440–1445 (2011).

697 38. Szyk, A., Deaconescu, A. M., Piszczek, G. & Roll-Mecak, A. Tubulin tyrosine ligase
698 structure reveals adaptation of an ancient fold to bind and modify tubulin. *Nat Struct Mol Biol*
699 **18**, 1250–1258 (2011).

700 39. Bowne-Anderson, H., Hibbel, A. & Howard, J. Regulation of Microtubule Growth and
701 Catastrophe: Unifying Theory and Experiment. *Trends Cell Biol* **25**, 769–779 (2015).

702